

Black-Hole Universe: Time Evolution

Chul-Moon Yoo,^{1,2,*} Hirotada Okawa,^{3,†} and Ken-ichi Nakao^{4,5,‡}

¹*Gravity and Particle Cosmology Group, Division of Particle and Astrophysical Science, Graduate School of Science, Nagoya University, Nagoya 464-8602, Japan*

²*Yukawa Institute for Theoretical Physics, Kyoto University, Kyoto 606-8502, Japan*

³*CENTRA, Departamento de Física, Instituto Superior Técnico, Avenida Rovisco Pais no 1, 1049-001 Lisboa, Portugal*

⁴*DAMTP, Centre for Mathematical Sciences, University of Cambridge, Wilberforce Road, Cambridge CB3 0WA, United Kingdom*

⁵*Department of Mathematics and Physics, Graduate School of Science, Osaka City University, 3-3-138 Sugimoto, Sumiyoshi, Osaka 558-8585, Japan*

(Received 19 June 2013; published 14 October 2013)

Time evolution of a black hole lattice toy model universe is simulated. The vacuum Einstein equations in a cubic box with a black hole at the origin are numerically solved with periodic boundary conditions on all pairs of faces opposite to each other. Defining effective scale factors by using the area of a surface and the length of an edge of the cubic box, we compare them with that in the Einstein–de Sitter universe. It is found that the behavior of the effective scale factors is well approximated by that in the Einstein–de Sitter universe. In our model, if the box size is sufficiently larger than the horizon radius, local inhomogeneities do not significantly affect the global expansion law of the Universe even though the inhomogeneity is extremely nonlinear.

DOI: [10.1103/PhysRevLett.111.161102](https://doi.org/10.1103/PhysRevLett.111.161102)

PACS numbers: 98.80.Jk, 04.25.D–

The effect of local inhomogeneity on the global expansion of the Universe has drawn much attention as one of fundamental issues in relativistic cosmology for many years. One remarkable work was done by Lindquist and Wheeler in 1957 [1]. In this work, they investigated the so-called “black hole lattice universe” composed of N cells ($N = 5, 8, 16, 24, 120, \text{ and } 600$) on the three sphere, each of which has a black hole at the center. Although the lattice universe is not an exact solution, with help from an intuitive idea, it is shown that the radius of the three dimensional sphere at maximum expansion asymptotes to that of the homogeneous and isotropic dust dominated the closed universe for a large value of N .

Recently, similar inhomogeneous universe models to the black hole lattice universe models have been investigated by using analytical or numerical techniques [2–8]. In this Letter, we numerically construct an expanding inhomogeneous universe model which is composed of regularly aligned black holes with an identical mass M , and compare the cosmic expansion rate of this inhomogeneous universe model with that of the homogeneous and isotropic universe. Hereafter, we call this inhomogeneous universe model the “black hole universe.”

In this Letter, we use the geometrized units in which the speed of light and Newton’s gravitational constant are one, respectively. The Greek indices represent spacetime components, whereas the small Latin indices represent spatial components.

The way to construct the initial data of the black hole universe is described in Ref. [7]. We briefly summarize it. We adopt the Cartesian coordinate system $\mathbf{x} = (x^1, x^2, x^3)$ and focus on a cubic region $-L \leq x^i \leq L$ ($i = 1, 2, 3$)

with a nonrotating black hole at the origin. We call the faces of this cubic box the *boundary* in this Letter. Because of the discrete symmetry, using conventional decomposition of the Einstein equations, we can reduce the constraint equations to three coupled Poisson equations with reflection boundary condition in the region $0 \leq x^i \leq L$. One of the equations is the Hamiltonian constraint equation for the conformal factor and the others are momentum constraint equations for longitudinal parts of the extrinsic curvature. To solve the equations, we need to fix the functional form of the trace part of the extrinsic curvature K . By the volume integral of the Hamiltonian constraint equation, we get an integrability condition which implies that there must be a domain with nonvanishing K . Since it is the simplest and the most convenient for our purpose to select K vanishing in the neighborhood of the origin, we adopt the following functional form of K :

$$K(\mathbf{x}) = -3H_{\text{eff}}W(R), \quad (1)$$

where H_{eff} is a positive constant which corresponds to the effective Hubble parameter, $R := |\mathbf{x}|$, and

$$W(R) = \begin{cases} 0 & \text{for } 0 \leq R \leq \ell \\ \sigma^{-36}[(R - \sigma - \ell)^6 - \sigma^6]^6 & \text{for } \ell \leq R \leq \ell + \sigma, \\ 1 & \text{for } \ell + \sigma \leq R \end{cases} \quad (2)$$

with ℓ and σ being constants which satisfy $\ell < \ell + \sigma < L$. An appropriate extraction of $1/R$ divergence of the conformal factor allows us to solve the coupled Poisson equations numerically. It should be noted that the value of H_{eff} must be determined so that the integrability condition

is satisfied, that is, we cannot freely choose the parameter H_{eff} but must appropriately fix the value during the numerical iteration. Since the results are not significantly dependent on ℓ and σ (we set $\ell = 0.1M$ and $\sigma = 1.8M$ in our calculation) the physical dimensionless parameter which characterizes the initial data is only L/M . In Ref. [7], we could get convergence for $1.4M \leq L \leq 10M$. We adopt the case $L = 2M$ as the initial data for the evolution in this Letter.

The numerical time evolution is followed by the COSMOS code which is an Einstein equation solver written in C++ by means of the BSSN formalism [9,10]. The algorithm is based on the SACRA code [11]. The 4th order finite differencing in space with unigrid and 4th-order time integration with a Runge-Kutta method in Cartesian coordinates are adopted in the COSMOS code. An apparent horizon solver based on Ref. [12] is implemented.

We write the line element of the spacetime as

$$ds^2 = -N^2 dt^2 + \gamma_{ij}(dx^i + \beta^i dt)(dx^j + \beta^j dt). \quad (3)$$

In order to determine the time slicing, we adopt the following condition:

$$\left(\frac{\partial}{\partial t} - \beta^i \frac{\partial}{\partial x^i}\right)N = -2N(K - K_c), \quad (4)$$

where K_c is the trace of the extrinsic curvature at the vertex $x^i = L$ ($i = 1, 2, 3$) at each time step. As for the spatial coordinates, we adopt the so-called hyperbolic gamma driver [13] with specific values of parameters given by

$$\frac{\partial \beta^i}{\partial t} = B^i, \quad (5)$$

$$\frac{\partial B^i}{\partial t} = \frac{\partial \tilde{\Gamma}^i}{\partial t} - \frac{3}{4M} B^i, \quad (6)$$

where $\tilde{\Gamma}^i := -\partial_j \tilde{\gamma}^{ij}$ with $\tilde{\gamma}^{ij} := e^{-4\psi} \gamma^{ij}$ and $\psi := (1/12) \ln(\det \gamma)$.

We define the cosmic expansion rate by using boundary variables on the geodesic slices [14] which is occasionally called constant proper time slices. In order to know the geometry of the boundary on the geodesic slices, we need to solve timelike geodesic equations on the boundary. 3 + 1 decomposition of geodesic equations is clearly described in Ref. [15]. Using the unit vector $n_\mu := -N \partial_\mu t$ normal to the time slices, we can decompose the unit tangent vector field of the timelike geodesic congruence as follows:

$$u^\mu = E(n^\mu + V^\mu), \quad (7)$$

where $V^\mu n_\mu = 0$. Let us represent a timelike geodesic by $x^\mu = x^\mu(t)$, where $t = x^0$. Then, we have [15]

$$\frac{dE}{dt} = EV^i(NK_{ij}V^j - \partial_i N), \quad (8)$$

$$\begin{aligned} \frac{dV^i}{dt} = & NV^j[V^i(\partial_j \ln N - K_{jk}V^k) + 2K_j^i - V^k \Gamma_{jk}^i] \\ & - \gamma^{ij} \partial_j N - V^j \partial_j \beta^i, \end{aligned} \quad (9)$$

where Γ_{jk}^i is the Christoffel symbol for the spatial metric γ_{ij} , and

$$\begin{aligned} \frac{d}{dt} &:= \frac{N}{E} u^\mu \frac{\partial}{\partial x^\mu} = N \left(n^\mu \frac{\partial}{\partial x^\mu} + V^i \frac{\partial}{\partial x^i} \right) \\ &= \frac{\partial}{\partial t} + (-\beta^i + NV^i) \frac{\partial}{\partial x^i}. \end{aligned} \quad (10)$$

The relation between the proper time τ and the time coordinate is given by

$$\frac{d\tau}{dt} = 1/u^0 = \frac{N}{E}. \quad (11)$$

The initial conditions for geodesic equations are given by $E = 1$, $V^i = 0$, and $\tau = 0$ in our simulation. It is sufficient for our purpose to consider the geodesics with $x^3 = L$ at $\tau = 0$. By the symmetry of this system, $x^3 = L$ and $V^3 = 0$ always hold. Solving Eqs. (8), (9), and (11), we obtain the proper time in the form of $\tau = f(t, x^A)$ ($A = 1, 2$). Then, the line element dl^2 of the boundary $x^3 = L$ on a hypersurface with a constant τ , i. e., a geodesic slice is given by

$$dl^2 = \left[(-N^2 + \beta^C \beta_C) \frac{\partial_A f \partial_B f}{(\partial_t f)^2} + \gamma_{AB} - \frac{2\beta_A \partial_B f}{\partial_t f} \right] dx^A dx^B. \quad (12)$$

We numerically obtain the proper area \mathcal{A} of the surface ($-L \leq x^A \leq L$, $x^3 = L$) and the proper length \mathcal{L} of the edge ($-L \leq x^1 \leq L$, $x^2 = L$, $x^3 = L$) by using this induced metric. Then, we define the effective scale factors as functions of the proper time as follows:

$$a_{\mathcal{L}}(\tau) := \mathcal{L}(\tau), \quad a_{\mathcal{A}}(\tau) := \sqrt{\mathcal{A}(\tau)}. \quad (13)$$

Since the coarse-grained black hole universe can be regarded as a homogeneous and isotropic universe model with vanishing spatial curvature by its construction, we compare the expansion rate of the black hole universe with that in the Einstein–de Sitter (EdS) universe. To compare the effective scale factors defined by Eq. (13) with that in the EdS universe, we define a fiducial scale factor. The general form of the scale factor in the EdS universe is given by

$$a_{\text{EdS}}(\tau) := a_f(\tau + \tau_f)^{2/3}. \quad (14)$$

Then we determine two parameters a_f and τ_f by the least-square fitting of this function with the numerical data in a reliable region of τ . Using this expression, the effective Hubble parameter is given by

$$H_{\text{EdS}}(\tau) = \frac{2}{3} \frac{1}{\tau + \tau_f}. \quad (15)$$

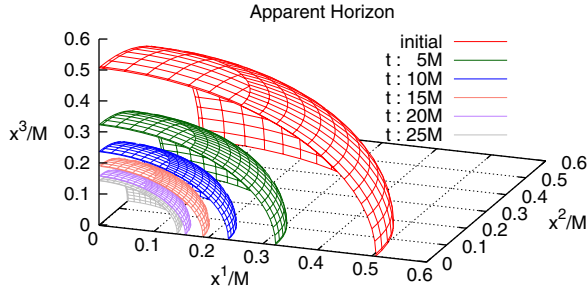


FIG. 1 (color online). Apparent horizon for each time step.

We performed the numerical simulation with four different resolutions: $R1$, $R2$, $R3$, and $R4$. The interval of coordinate grids for each numerical run is given by $\Delta x/M \approx 4/59, 4/91, 4/123$ and $4/155$ for $R1, R2, R3$, and $R4$, respectively.

Before showing the results of effective scale factors, we note the resolution of the apparent horizon and constraint violation. At the initial moment, an almost spherical apparent horizon with the coordinate radius $R \approx 0.5M$ exists. As shown in Fig. 1, the coordinate radius of the apparent horizon decreases as it evolves.

At some time, our apparent horizon finder fails to find out the horizon because of the limitation of the resolution. For $R4$, it happens at $t \sim 25M$. While the horizon can be found, variation of the horizon area is smaller than 0.1%, which is the same order as the typical fraction of violation of the Hamiltonian constraint as is shown below. This implies that the horizon area is constant in time within our numerical precision.

As is shown in Fig. 2, after the failure in the apparent horizon search, the violation of the Hamiltonian constraint propagates outward, and the reliable region becomes narrower as time goes on. However, the numerical computation does not crash and we can proceed with the calculation. Even after the size of the apparent horizon

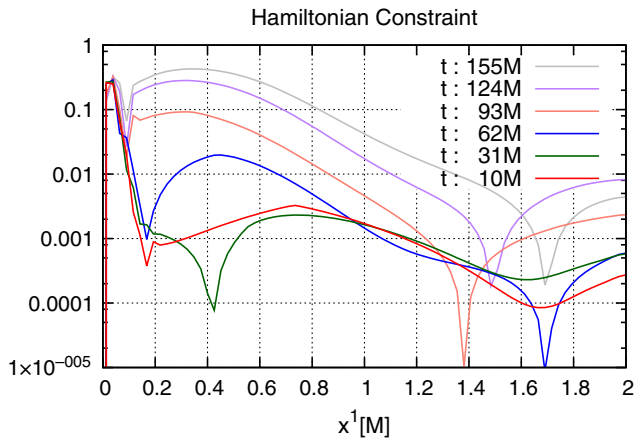


FIG. 2 (color online). Evolution of the violation of the Hamiltonian constraint on the x^1 axis for $R4$. Zero means no violation whereas one corresponds to the largest violation.

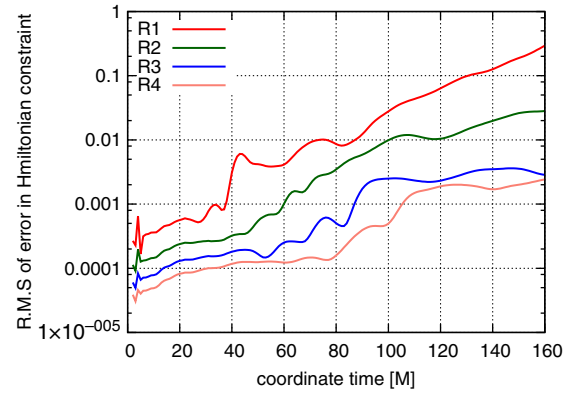


FIG. 3 (color online). Root-mean square of the errors in the Hamiltonian constraint at grid points on the boundary.

becomes too small to be resolved, the spacetime in the vicinity of the boundary is simulated with sufficient accuracy, since the present numerical results on the behaviors of the effective scale factors pass the convergence test. In order to show the convergence clearly, we depict the root-mean-square value of errors in the Hamiltonian constraint at grid points on the boundary in Fig. 3. It is seen from this figure that the error reduces with higher spatial resolution. In the beginning of the simulation, we find accurate second order convergence that the error scales to Δx^2 . This is because the initial data sets are given by the 2nd order successive-over-relaxation method for each resolution [7], although the evolution code has the 4th order accuracy.

In Fig. 4, we show the effective scale factors as functions of the proper time. The fiducial scale factor $a_{\text{EdS}}(\tau)$ determined by fitting with $R4$ is also shown. The fitting is done in the region $20M < \tau < 60M$, in which the results of all runs almost coincide with each other. The given value of parameters are $a_f \approx 2.64M$ and $\tau_f \approx -3.25M$. We also show the deviation of the effective scale factors from $a_{\text{EdS}}(\tau)$ in Fig. 5. It can be found from Figs. 4 and 5 that the behavior of the effective scale factors for $R4$ is well

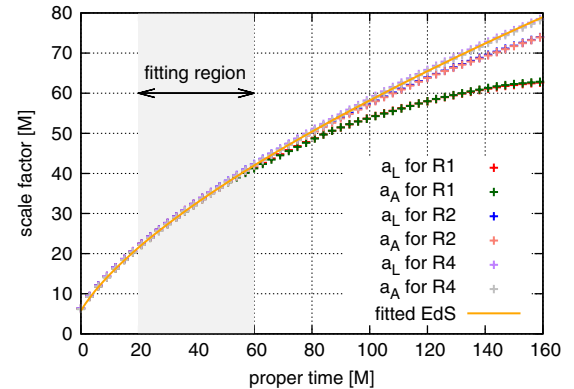


FIG. 4 (color online). Effective scale factors and a_{EdS} as functions of τ . $a_{\mathcal{A}}$ almost overlaps $a_{\mathcal{L}}$.

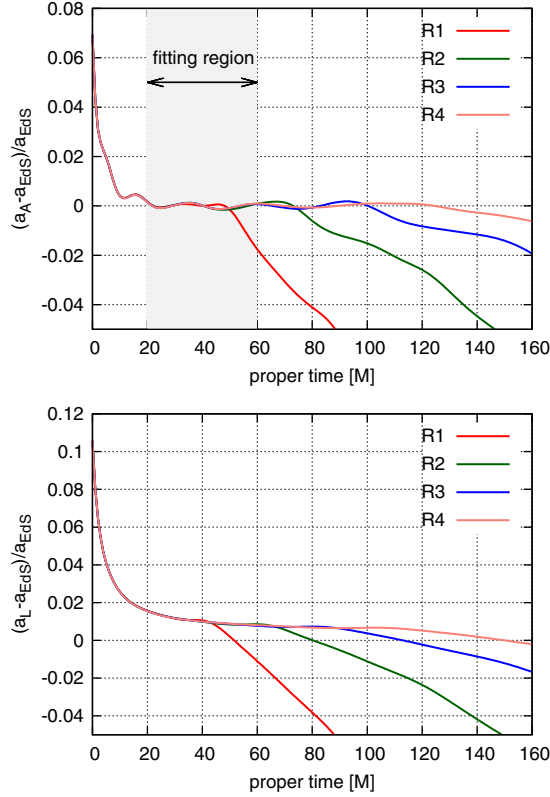


FIG. 5 (color online). Deviation of the effective scale factors a_A and a_L from a_{EdS} for each resolution.

approximated by that of the EdS universe in the shown period of τ except for a short period in the beginning. This result is consistent with the suggestion given by the numerical simulation of the collapsing eight-black-hole lattice [5] and an initial data sequence [7].

It is worth noting the reason why we have defined the effective scale factor by Eq. (13). The reason is that, since the total volume inside the box is infinite, it is hard to define the volume average in a physically meaningful manner. Therefore, we do not use the spatial volume average to define the effective scale factor differently from other many related works (see, e.g., Ref. [16] and references therein).

The number of black holes N_{BH} inside the Hubble radius H_{EdS}^{-1} is given by

$$N_{\text{BH}} \sim \frac{1}{M} \times \frac{4\pi}{3} H_{\text{EdS}}^{-3} \times \frac{3}{8\pi} H_{\text{EdS}}^2 = \frac{H_{\text{EdS}}^{-1}}{2M} = \frac{3}{4} \frac{\tau + \tau_f}{M}, \quad (16)$$

and we obtain $N_{\text{BH}} \sim 100$ for $\tau \sim 130M$. As was discussed in Ref. [7], it is expected that the deviation of the black hole universe from the EdS one becomes the smaller, the larger N_{BH} becomes; or, in other words, the effects of local

inhomogeneities on the global expansion law are negligible if N_{BH} is sufficiently large. If so, the expansion law of the black hole universe will approach to that of the EdS universe as it expands, and the present result supports this expectation.

The universe model studied here is highly idealized, since this work is the first step in the study of the Universe dominated by black holes. Generalizations of our toy model to that with varieties of mass and separation, etc., and the dependence of the results on them are still open issues which should be clarified in the future.

We thank M. Sasaki for encouraging us to work on this subject, and M. Shibata for helpful discussions and comments. We also thank T. Hiramatsu for technical support in the numerical computations. The numerical calculations were partly carried out on SR16000 at YITP in Kyoto University. This work was supported in part by JSPS Grant-in-Aid for Scientific Research (C) (No. 21540276 and No. 25400265).

*yoo@gravity.phys.nagoya-u.ac.jp

†hirotada.okawa@ist.utl.pt

‡knakao@sci.osaka-cu.ac.jp

- [1] R. W. Lindquist and J. A. Wheeler, *Rev. Mod. Phys.* **29**, 432 (1957).
- [2] T. Clifton and P. G. Ferreira, *Phys. Rev. D* **80**, 103503 (2009).
- [3] T. Clifton, K. Rosquist, and R. Tavakol, *Phys. Rev. D* **86**, 043506 (2012).
- [4] J.-P. Uzan, G. F. Ellis, and J. Larena, *Gen. Relativ. Gravit.* **43**, 191 (2011).
- [5] E. Bentivegna and M. Korzynski, *Classical Quantum Gravity* **29**, 165007 (2012).
- [6] J.-P. Bruneton and J. Larena, *Classical Quantum Gravity* **29**, 155001 (2012).
- [7] C.-M. Yoo, H. Abe, Y. Takamori, and K. I. Nakao, *Phys. Rev. D* **86**, 044027 (2012).
- [8] E. Bentivegna, [arXiv:1305.5576](https://arxiv.org/abs/1305.5576).
- [9] M. Shibata and T. Nakamura, *Phys. Rev. D* **52**, 5428 (1995).
- [10] T. W. Baumgarte and S. L. Shapiro, *Phys. Rev. D* **59**, 024007 (1998).
- [11] T. Yamamoto, M. Shibata, and K. Taniguchi, *Phys. Rev. D* **78**, 064054 (2008).
- [12] M. Shibata, *Phys. Rev. D* **55**, 2002 (1997).
- [13] M. Alcubierre, B. Brügmann, P. Diener, M. Koppitz, D. Pollney, E. Seidel, and R. Takahashi, *Phys. Rev. D* **67**, 084023 (2003).
- [14] L. Smarr and J. W. York, Jr., *Phys. Rev. D* **17**, 2529 (1978).
- [15] F. H. Vincent, E.ourgoulhon, and J. Novak, *Classical Quantum Gravity* **29**, 245005 (2012).
- [16] S. Rasanen, *Classical Quantum Gravity* **28**, 164008 (2011).